



Grant Agreement No. 783169
U-Geohaz – “Geohazard impact
assessment for urban areas”

Deliverable D3.8: VEW validation report

A deliverable of WP 3: Early Warning System for Volcanic Activity

Due date of deliverable: 30/06/2019
Actual submission date: 26/07/2019

Lead contractor for this deliverable: IGME, CNIG-IGN, SCP and GOBCAN

Dissemination Level		
PU	Public	
PP	Restricted to other programme participants (including the Commission Services)	
RE	Restricted to a group specified by the Consortium (including the Commission Services)	
CO	Confidential, only for members of the Consortium (including the Commission Services)	
TN	Technical Note, not a deliverable, only internal for members of the Consortium	

Table of Content

EXECUTIVE SUMMARY	3
REFERENCE DOCUMENTS	4
1 INTRODUCTION.....	6
2 TEST SITE DESCRIPTION.....	7
2.1 El Hierro Island.....	7
3 METHODS	9
3.1 Methodology for InSAR products validation with GNSS.....	9
3.1.1 Validation procedure.....	10
3.2 Phase splitting methodology applied to 6-12 days wrapped interferograms. Validation for volcano monitoring.....	12
4 RESULTS	13
4.1 Validation of VEW-DAM	13
4.2 Phase splitting results.	18
5 POSSIBLE IMPROVEMENTS	20
REFERENCES.....	20

EXECUTIVE SUMMARY

The tasks performed in Activity 3.5 named “VEW Validation” and lead by IGME and CNIG-IGN are reported in this document, which represents the fourth official deliverable of WP3 “Early Warning System for Volcanic Activity”. The main goal of this activity is the validation of the VEW and DAM generated in 3.3 and 3.4 for El Hierro Island. The test site includes Tenerife, La Palma and el Hierro Islands. However, we have focused all the validation activities on el Hierro because is where we have tested different approaches. For this validation we have compared the Deformation Activity Map of El Hierro Island with GNSS time series during the same time interval (May 2017 – August 2018). Since no deformation was detected in the island during this period the results have not been compared with previous existing geohazard maps. We have determined the confidence degree of the generated maps and identify sources of uncertainties. We finally propose possible improvements.


REFERENCE DOCUMENTS

N°	Title
RD1	DoW U-Geohaz
D3.1	User Requirements
D3.2	VEW Assessment Procedure
D3.4	Description of Volcanic Early Warning System (VEW)
D3.5	Updated Deformation Activity Map (V0)

CONTRIBUTORS

Contributor(s)	Company	Contributor(s)	Company
Marta Béjar Pizarro	IGME	Elena González Alonso	CNIG-IGN
Gerardo Herrera	IGME	Anselmo Fernández García	CNIG-IGN
Roberto Sarro	IGME	Sergio Ligüerzana Rodríguez	CNIG-IGN
Rosa María Mateos	IGME	Laura García Cañada	CNIG-IGN
Anna Barra	CTTC	Jose Navarro	CTTC

REVIEW: CORE TEAM

Reviewed by	Company	Date	Signature
Oriol Monserrat	CTTC	25/07/2019	

1 INTRODUCTION

Currently, 800 million people live within 100 km of a volcano that has the potential to erupt (Loughlin et al., 2015). Volcanic eruptions can have devastating economic and social consequences for volcanically vulnerable areas and thus properly forecast volcano hazards is essential to reduce their impacts on people and infrastructure. Fortunately, many eruptions are preceded by volcanic unrest that can be detected using monitoring tools such as seismometers, GPS, gas sampling instruments, and spaceborne remote sensing.

An Early Warning System (EWS) can be defined as a system designed to provide “hazard monitoring, forecasting and prediction, disaster risk assessment, communication and preparedness activities, systems and processes that enables individuals, communities, governments, businesses and others to take timely action to reduce disaster risks in advance of hazardous events” (UN 2003). Volcano EW systems are used globally to communicate volcano-related information to diverse stakeholders ranging from specific user groups to general public, or both (Potter et al. 2018). VEW can be based on thresholds of single parameters (e.g. GPS, tilt, strain-meter, seismic) or use combination of several mono-parametric data acquired from multiple sensors or synthesis of different parameter acquired by multiple sensors. Within the framework of a volcano EW system, Volcano Alert Level (VAL) systems are commonly used as a simple communication tool to inform society about the status of activity at specific volcanoes.

Ground deformation at volcanoes can be produced by a variety of processes including dyke intrusions and propagation, opening or closing of volcanic vents, inflation of deep or shallow magma reservoirs and deflation episodes (e.g. Biggs and Pritchard 2017, Dzurusin 2003). Although unrest episodes may or may not lead to eruption, volcanic deformation have a significant statistical link to eruption (Biggs et al., 2014). Therefore, detecting and monitoring surface deformation on active volcanoes is key to identify unrest episodes and can give information about the depth and geometry of the magma source.

Interferometric Synthetic Aperture Radar (InSAR) is a satellite remote sensing technique particularly well adapted for volcano monitoring because it can detect ground displacement at the centimetre scale over large geographic areas, including volcanoes in remote and inaccessible regions with no ground-based monitoring (Garthwaite et al. 2019, Biggs et al., 2014, Biggs & Pritchard, 2017; Pinel et al., 2014).

The main goal of WP3 is to implement an Early Warning System based mainly on the exploitation of Deformation Activity Maps derived from Sentinel-1 data with a 6-day temporal repeatability. For this purpose, DIM (Displacement Maps) and DAM (Deformation Activity Maps) are integrated with other deformation data (GPS, tiltmeters) in order to reinforce the early warning system of volcanic activity. This deliverable describes the methodology and results of the VEW and DAM validation.

This document is organized as follows: we first describe the test site (section 2) and the methodology used to validate the VEW-DAM and the method for phase splitting applied to 6-12 days wrapped interferograms (section 3). Then we present the results regarding the VEW validation and we assess the confidence degree and uncertainty (section 4.1). We finally discuss the possible improvement of the system (section 4.2)

2 TEST SITE DESCRIPTION

2.1 El Hierro Island

El Hierro is an oceanic island situated at the south-western point of the Canary Islands, Spain (See Figure 2-1). With an area of 268 km² and a population of 10.679 inhabitants (Instituto Nacional de Estadística (INE) 2018), the island has three municipalities, Frontera, El Pinar and Valverde, where the capital is located. The island is the emergent summit of a volcanic shield which rises from a depth of 3700-4000 m. The characteristic trilobate form of the island is similar to that of other oceanic islands with three very marked directions (Martí et al. 1996; Carracedo et al. 2001). The island rifts form topographic ridges at angles of 120°, oriented in NW, NE and S directions. The maximum elevation is 1501 meters, which contributes to provide El Hierro with the higher average slopes of the Canary Islands.

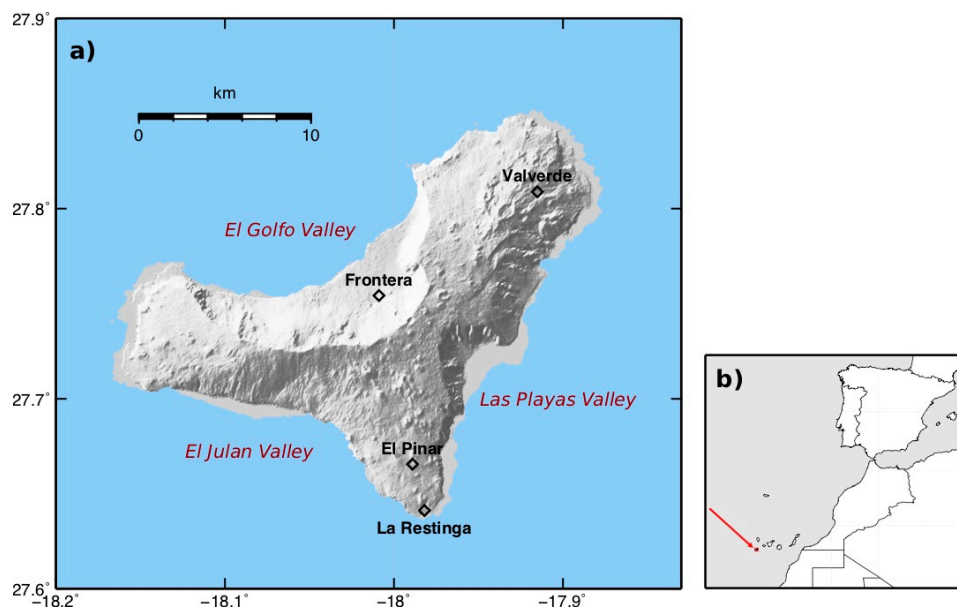


Figure 2-1 Elevation map of El Hierro island (1-arc-s digital elevation model from the Shuttle Radar Topography Mission). The inset map (b) shows the location of the island with a red arrow.

There are basically two theories about The Canary Island origin. One of them states that the Canary Islands originated in the early Miocene when the African plate moved slowly over a mantle hotspot (Schmincke 1982, Morgan 1972). Unlike the Hawaiian Islands, the Canary Islands do not follow a simple age progression, although there is a general evolution from the oldest volcanic rocks of Fuerteventura in the east (>20 Ma) to El Hierro in the west (<2 Ma). La Palma and El Hierro, the westernmost islands, are both younger than 2 Ma indicating both that the focus of the present-day hotspot activity is located in this region and that the island chain is extending towards the west. Alternative hypotheses support a propagating fracture connecting the archipelago and African Atlas Mountains, compression-related tectonic uplift and local rifting in the islands (Anguita, 2000).

Most of the landforms of El Hierro have been generated by a combination of constructive and destructive volcanic processes. From a geological point of view, El Hierro can be divided into three volcanic cycles that correspond to three successive volcanic edifices (Becerril et al. 2013 and references therein) : the Tiñor Edifice (1.12–0.88 Ma), the El Golfo-Las Playas Edifice (545–176 ka), and the Rifts Volcanism (158 ka–present). These three volcanic phases are separated by important tectonic events.

El Hierro has experienced rapid growth and destructive events in its 1.12 million years history. At least four giant landslides (El Golfo, El Julan, San Andres, and Las Playas) have modified ~ 450 km³ of El Hierro during the last 200–300 thousand years. Each landslide event has removed around 3% of the total edifice volume. The extent of landsliding indicates that it is the main process of decay (Gee et al. 2001). The El Golfo landslide is the most recent (15 ka), best described and clearly defined landslide in the Canary Islands. It is characterized by a very high sea cliff (up to 1000 m in height) surrounding the Frontera valley.

Regarding volcanic events in El Hierro Island, Becerril et al. (2015) estimates as a minimum one eruption every 1000 years. In the last 600 years no historical eruptions had been documented apart from a seismic crisis in 1793 (Darias y Padrón, 1929). In 2011, after more than 200 years of quiescence, a shallow water eruption occurred off the coast of La Restinga village (Figure 2-1), in the south of the island (Meletlidis et al. 2015). The eruption lasted five months and was preceded by three months of intense seismic activity (López et al. 2012). The eruption was driven by the ascent of a mantle-derived magma initially accumulated in a reservoir located at ~ 20 –25 km depth below the island that progressively accumulated in the lower crust before the final ascension to the eruption site (Martí et al. 2013, García et al. 2014, Longpré et al. 2014, Meletlidis et al. 2015). After the end of the eruption in March 2012, several magmatic intrusions were detected underneath the island in the period June 2012 to March 2014 (Benito-Saz et al. 2017). Afterwards, only occasional seismic activity has been detected.

3 METHODS

3.1 Methodology for InSAR products validation with GNSS

After volcanic unrest episode in 2004 at Tenerife Island, IGN was commanded by law to hold responsibilities on volcanic monitoring management in Spain, communication and determination of associated hazards. According to this aim, a multi-parametric network of stations was deployed and maintain in the Canary Islands.

Deformation is one of the main precursors of a volcanic eruption. Currently IGN operates a network of 28 GNSS stations, supported by data collected from other public networks, as IGS and GRAFCAN GNSS permanent ones (<https://www.ign.es/web/ign/portal/vlc-gps>).

In El Hierro, IGN network is comprised of six stations uniformly distributed along the island.

Since 2007, GNSS time series have been generated and analysed daily in the Canary Islands. This procedure has allowed us to study background movements of some GNSS stations and seasonal effects. It was also able to detect the volcanic unrest on El Hierro Island in 2011, which ended in a submarine eruption, and the 2012-2014 post-eruption volcanic activity (López C. et al., 2012; Klügel et al., 2015).

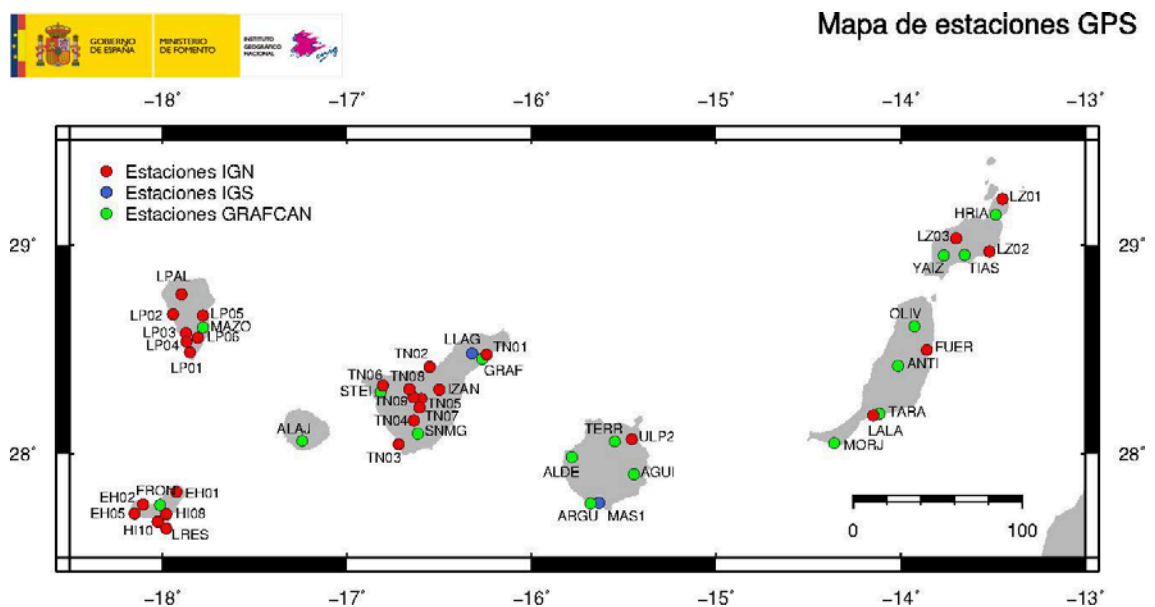


Figure 3-1 GNSS permanent networks in Canary Islands.

In this section we describe the criteria adopted to validate the Deformation Activity Map, the U-GEOHAZ product created with Sentinel-1 images and included in deliverable D3.5, using time series analyses from the IGN-GNSS networks. Final and daily NEU (north, east, up) coordinates with tectonic plate movement removed, will be used for the validation. For further details on GNSS processing approach for volcano monitoring see García-Cañada et al., 2013.

3.1.1 Validation procedure

GNSS time series

1. **GNSS-NEU time series:** Generation of GNSS-NEU time series for the selected time interval and estimation of velocities by linear regression.
2. **GNSS-NEU time series projection to LOS:** To be able to compare InSAR and GNSS time series, GNSS-NEU time series need to be projected into the line-of-sight (LOS) direction (*Hanssen, 2001*):

$$d_r = d_u \cos(\theta_{inc}) \left[d_n \cos\left(\alpha_h - \frac{3\pi}{2}\right) + d_e \sin\left(\alpha_h - \frac{3\pi}{2}\right) \right]$$

According to the Sentinel-1 ascending orbits used in this analysis, these parameters are:

- d_r : deformation vector in LOS direction
 - d_n, d_e, d_u : deformation vectors in north, east and up directions coming from GNSS-NEU time series
 - θ_{inc} : incidence angle for the area of interest (between 27.°53 and 44°28, depending on the island)
 - α_h : orbit heading (~12.5°)
3. **Velocity estimation of the GNSS-LOS time series:** According to the observed trends at GNSS-NEU time series, we decide to use a common least squares approach to estimate velocities for the projected time series.
 4. **Interpretation of GNSS-LOS deformations:** According to projected time series and estimated velocities, we perform a first interpretation of the results. A GNSS station with a velocity above two times de standard deviation of the adjustment is considered an active GNSS-LOS candidate. On the other hand, stations with a velocity below two times de standard deviation of the adjustment is considered a stable GNSS-LOS candidate.

InSAR time series

5. **Area selection around GNSS station:** instead of selecting the time series of the closer measured points (MP) to the GNSS station, we decide to select an area of a certain size around the GNSS station and study the behavior of the MP included on it.

An equal-size-area or an equal-number-of-pixel criterion can be used to choose the area size. In both cases, a significant number of pixels are mandatory to obtain a representative behavior of the area.

We perform some tests to find a suitable radius for the area, always larger than the MP size, $\cong 40 \text{ m} \times 40 \text{ m}$ after multilooking. In this case, we finally decided to use an equal-area criterion of 350 m radius around each GNSS station.

6. **Analysis of the MP behavior and final area selection:** Time series for every MP inside selected areas around GNSS stations are generated and analyzed. Two situations can occur:

- a. MP in the area show the same behavior: area is well selected and we can proceed to calculate an average to work with. We also estimate velocities using same approach as in (3).
- b. MP in the area show different behavior: the area needs to be reduced until we observe all the MP have the same behavior (a).

If after successive reductions, we still observe the same behavior we consider that the area is noisy and we discard the point for the analysis.

7. **Interpretation of InSAR deformations:** According to the averaged deformations obtained, we perform a first interpretation of the results. Deformation areas with a velocity above 12 mm/yr are considered an active InSAR candidate. On the other hand, areas with a deformation velocity below 12 mm/yr, are considered stable InSAR candidate. This threshold corresponds to twice the standard deviation of all the measured points. This criterion has been selected according to Barra A. et al, 2017.

Validation

8. **Validation of InSAR with GNSS-LOS time series:** according to criteria established in (4) and (7), we compare both time series. The following situations can take place:

Cases	A. InSAR deformation	B. InSAR no deformation
A. GNSS-LOS deformation	AA. VALIDATED	AB. NO VALIDATED
B. GNSS-LOS no deformation	BA. NO VALIDATED	BB. VALIDATED

Table 3-1 Validation cases.

- **Case AA:** Significant deformations are observed in both GNSS-LOS and InSAR time series. Acceptable differences between both in magnitude and velocity can take place attending to different noises of the time series.
- **Case AB:**
Possible causes:
 - Small deformations could be detected in the GNSS-LOS time-series but not in the InSAR time series as being the latter generally noisier.
 - GNSS-LOS deformation is punctual and selected MP included in the 350 meters area around the station do not represent the real movement of the station.
- **Case BA**
Possible causes:
 - As GNSS measures punctual deformations it is possible that the station itself is not suffering movements but the 350 meter radius area around it does.
- **Case BB:** No significant deformation is observed in GNSS-LOS or InSAR time series, regardless of the noise of the series.

In case the validation is still unclear we can make use of:

- IGN-GNSS complete time series generated in El Hierro since 2011.
- External information (as land use map, rockfall inventory map, element at risk catalogue and damage events database).
- Field campaigns, if necessary.

3.2 Phase splitting methodology applied to 6-12 days wrapped interferograms. Validation for volcano monitoring

During the generation of the second delivery of U-Geohaz project, an algorithm based on the direct integration of consecutive images has been used. In this approach, a phase splitting process is applied to the wrapped differential interferograms in order to separate high and low frequencies. After the application of the spatial filter, two different products are obtained: a wrapped high-frequencies (HF) interferogram and a wrapped low-frequencies (LF) interferogram.

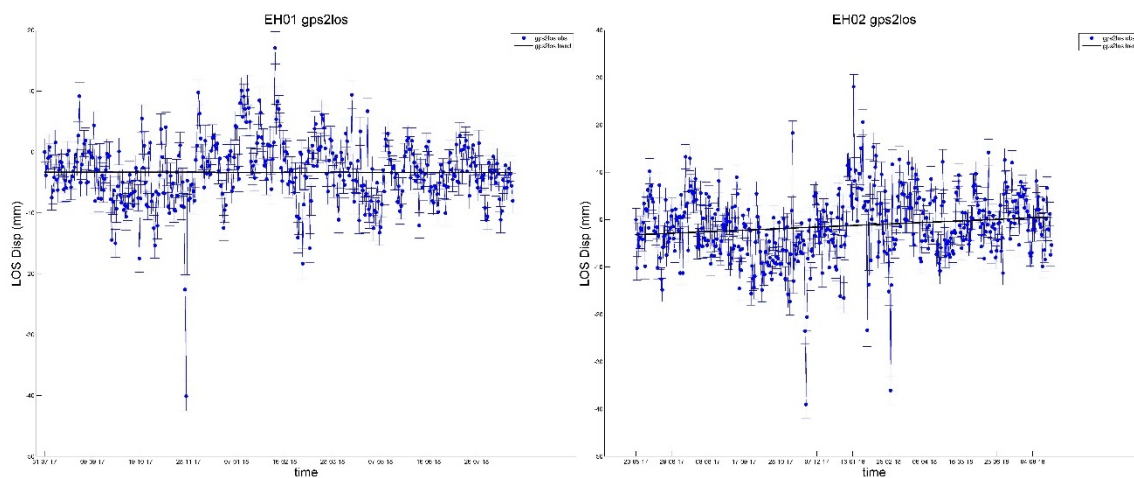
The HF products contain local deformation and topographic effects. Otherwise, LF product contains non local deformation and atmospheric effects. These new products help the experts in the analysis and interpretation of the 6-12 days interferograms and can be very useful for the interferogram interpretation during volcanic unrests. Most of the deformation associated with these unrest episodes is expected to be contained in the LF interferogram.

In addition, the subtraction of noise from the LF interferograms, improve the result of the phase unwrapping process.

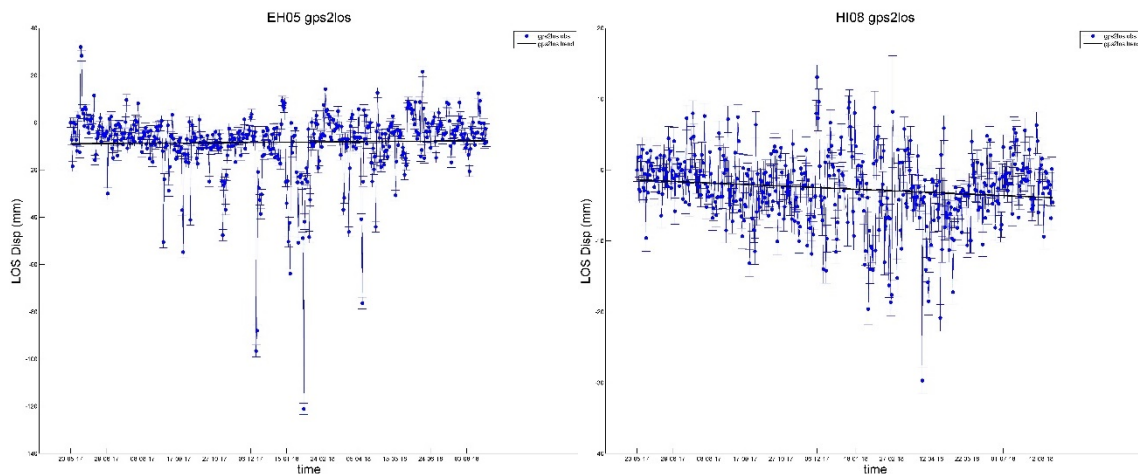
4 RESULTS

4.1 Validation of VEW-DAM

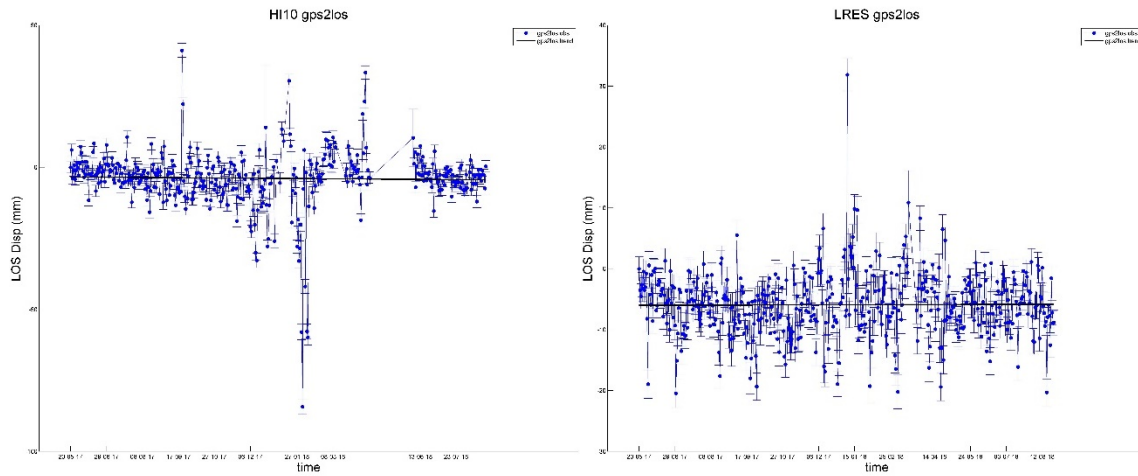
According to the criteria explained in 3.2.2, all GNSS-LOS are STABLE during 20 May 2017 and 25 August 2018. See the following pictures where the complete GNSS-LOS series for the selected period are represented.



Figures 4-1 and 4-2 EH01 and EH02 time series projected to LOS

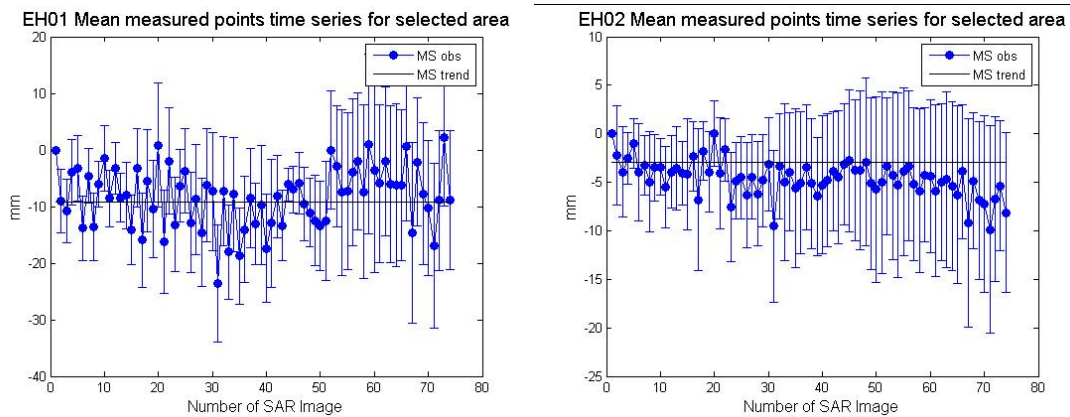


Figures 4-3 and 4-4 EH05 and HI08 time series projected to LOS

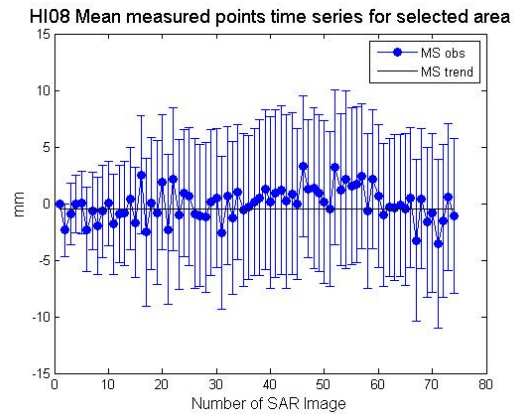
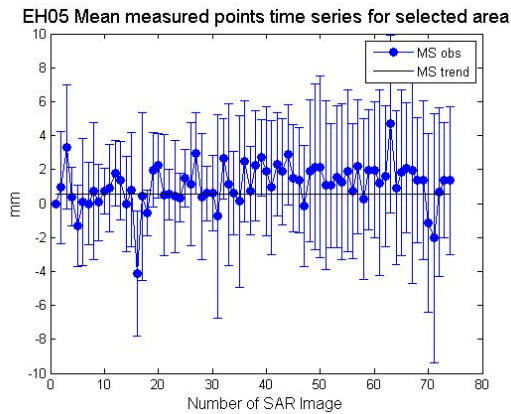


Figures 4-5 and 4-6 HI10 and LRES time series projected to LOS

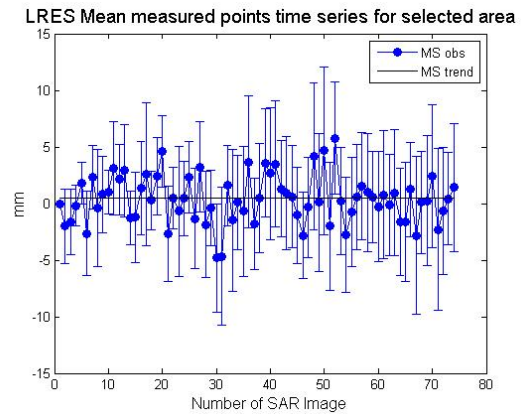
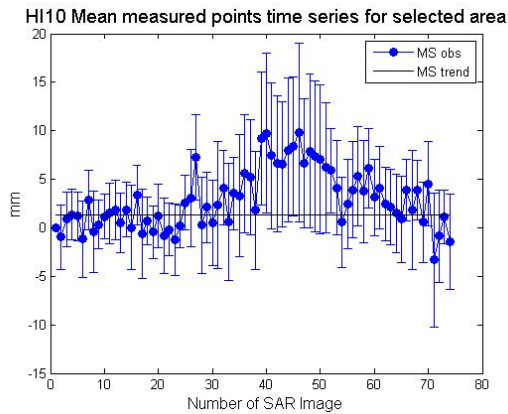
In the same way, for DAM, there are not ACTIVE areas around any GNSS station. See the following pictures where the mean measured points time series for the selected areas are represented.



Figures 4-7 and 4- 8 EH01 and EH02 mean measured points time series for selected areas



Figures 4-9 and 4-10 EH05 and HI08 mean measured points time series for selected areas



Figures 4-11 and 4-12 HI10 and LRES mean measured points time series for selected areas

Validation.

Taking into account Table 3-1, we are in case BB which means that significant deformation is not observed in GNSS-LOS or measured points time series, so DAM is successfully validated.

See the following pictures where GNSS-LOS and InSAR time series are compared. The GNSS-LOS time series have been replaced by a seven days mean solution centered in the date of the SAR acquisition. This mean has been computed removing coarse errors considering as such those with a distance to the mean greater than two times the standard deviation for the considered period.

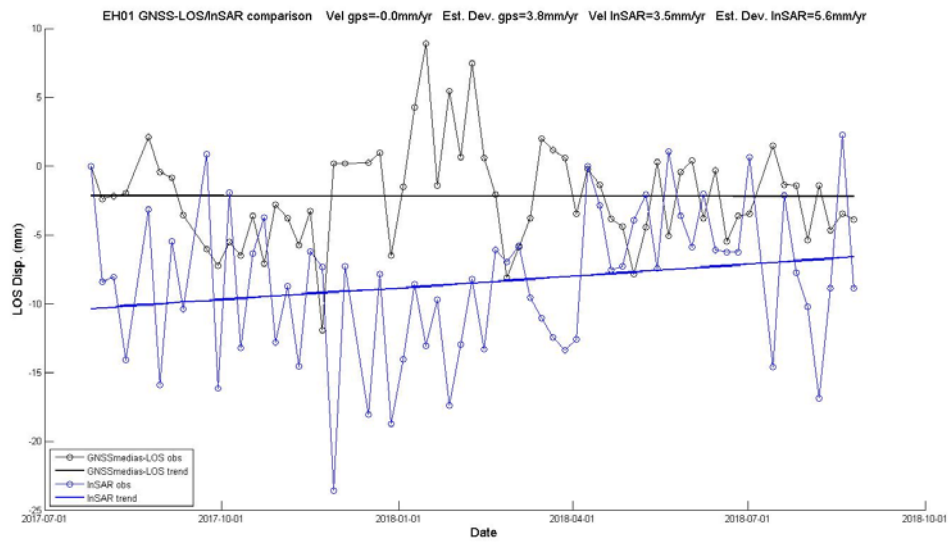


Figure 4-13 EH01 GNNS time series projected to LOS / InSAR comparison.

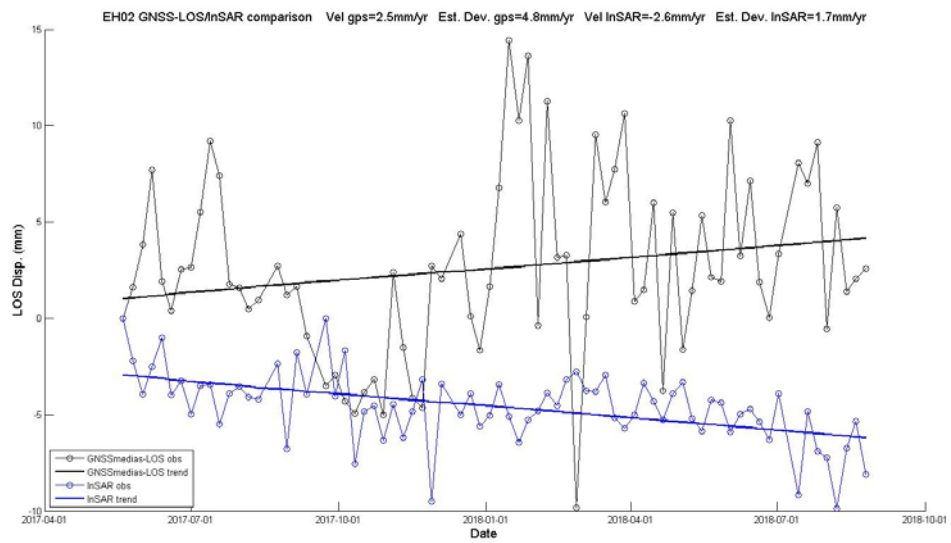


Figure 4- 14 EH02 GNNS time series projected to LOS / InSAR comparison.

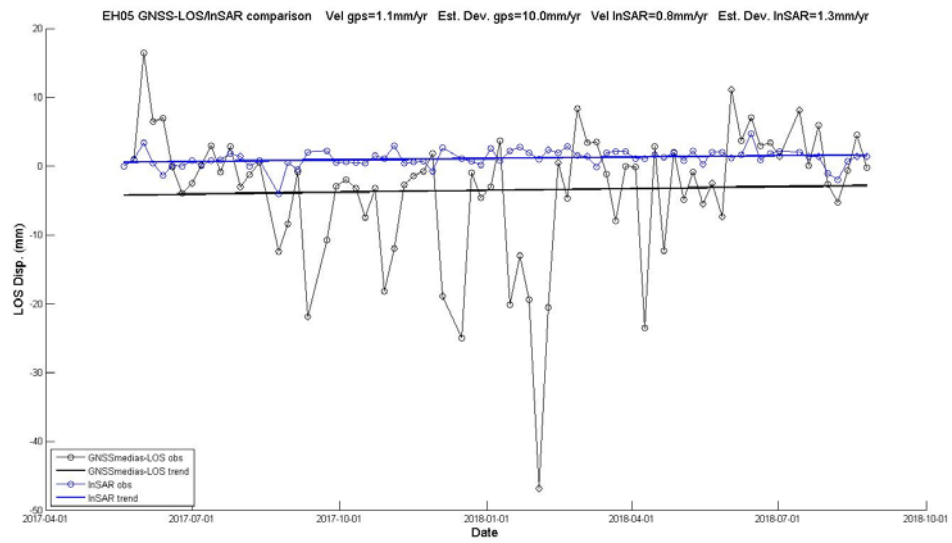


Figure 4-15 EH05 GNNS time series projected to LOS / InSAR comparison.

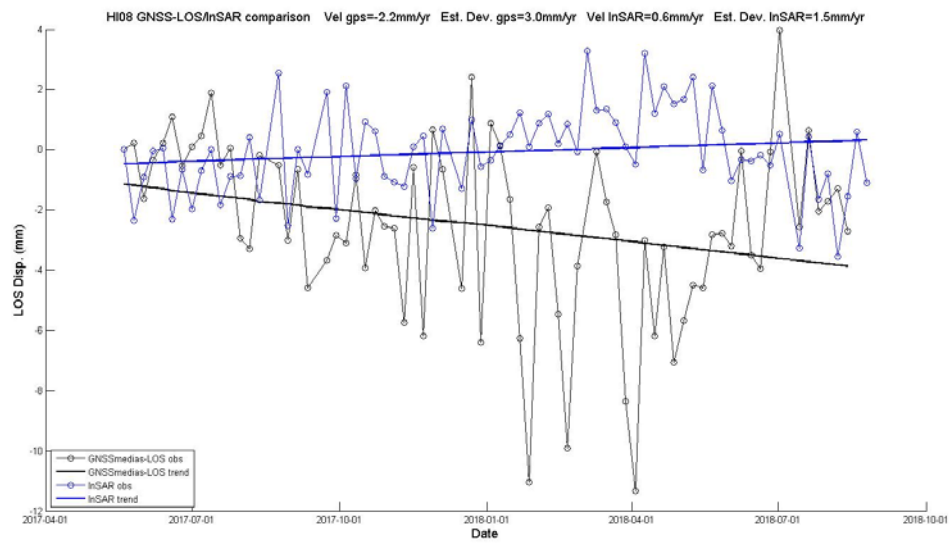


Figure 4-16 H108 GNNS time series projected to LOS / InSAR comparison.

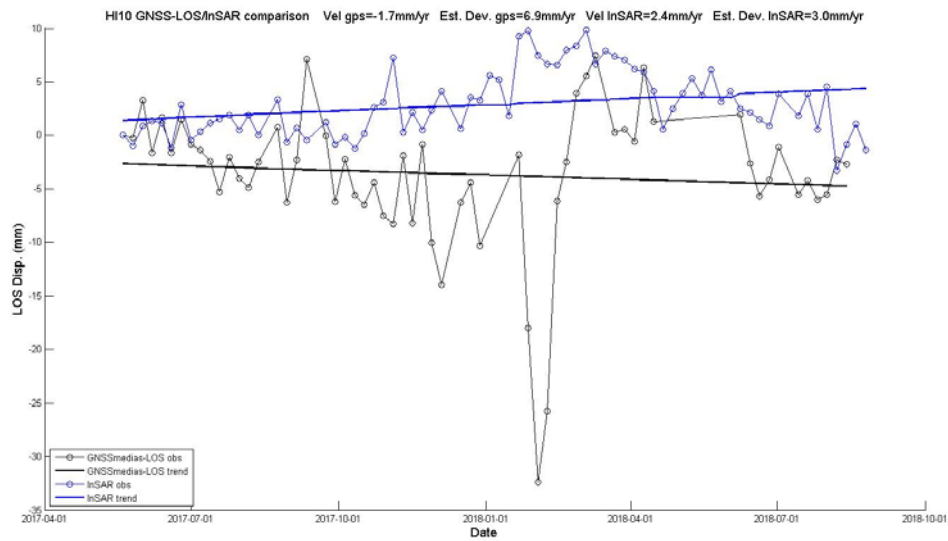


Figure 4-17 HI10 GNNS time series projected to LOS / InSAR comparison.

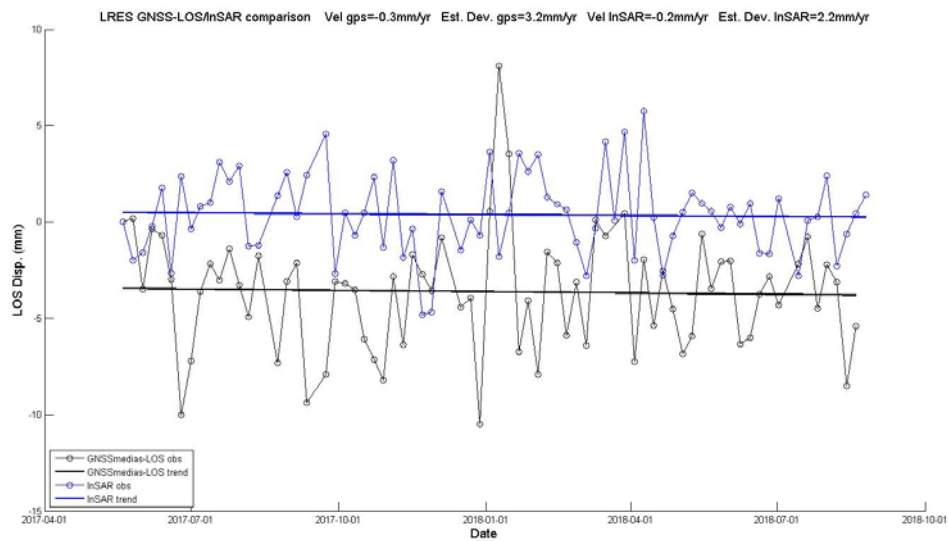


Figure 4-18 LRES GNNS time series projected to LOS / InSAR comparison.

4.2 Phase splitting results.

As it was explained in 3.2. after the phase splitting process, we obtained two different products: a wrapped high-frequencies (HF) interferogram and a wrapped low-frequencies (LF) interferogram.

The Figure 4-19 shows an interferogram from El Hierro corresponding to the unrest process occurred on the island in 2011.

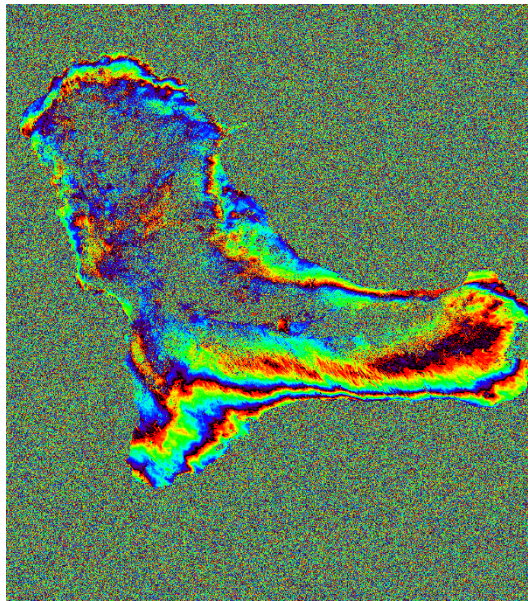


Figure 4-19 El Hierro interferogram

In the HF interferogram (Figure 4-20) are contained mainly noisy points (most correspond to vegetated areas), but also local deformations and topographic effects. By contrast, the LF interferogram (4-21) shows non local deformation and atmospheric effects.

As we can see, in the LF interferogram is much more cleaned of noisy points, what supposes an important improvement in the phase unwrapping.

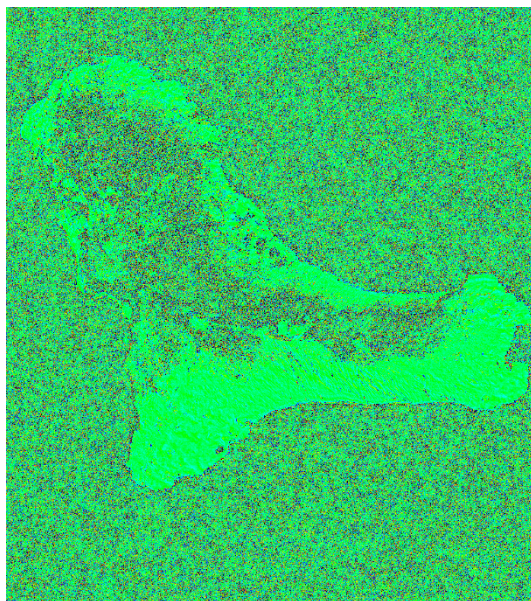


Figure 4-20 HF interferogram

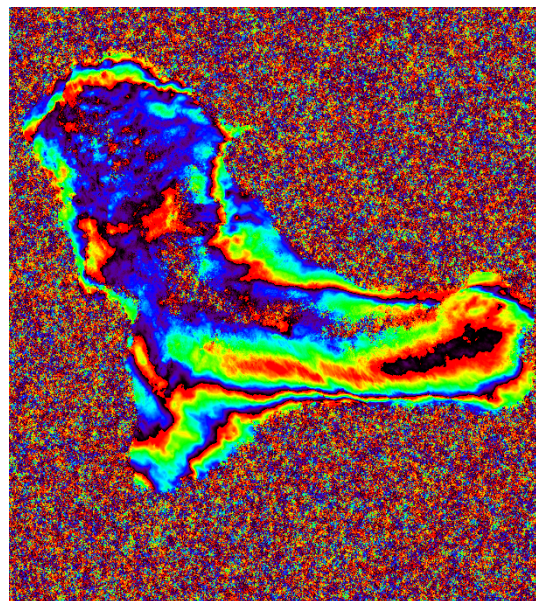


Figure 4-21 LF interferogram

5 POSSIBLE IMPROVEMENTS

The method proposed here based on the spatial filtering of 6-12 days interferograms can be very useful to detect volcanic ground deformation during unrest periods. As explained in methods, we expect most of the volcanic deformation to be contained in the LF interferogram. However, this interferogram may also contain atmospheric effects that are usually produced by topographically correlated phase delay due to variations in concentration of stratified water vapour (e.g. Doin et al., 2009; Hanssen, 2001). When interpreting individual interferogram over active volcanoes, it is not easy to distinguish these atmospheric signals from volcanic deformation because a similar pattern (correlation between height of topography and phase) can be produced by injection or drainage of a body of magma below a volcanic edifice. A possible improvement of the methodology proposed here would be to remove the LF atmospheric contribution from our interferograms. For that purpose, different methods have been proposed, including empirical approaches based on the local correlation between the phase delay and the topography (e.g. Béjar-Pizarro et al. 2013), numerical weather models (E.g. ECMWF, Walters et al., 2013) and Global Positioning System data (e.g. Li et al., 2006). New services such as the Generic Atmospheric Correction Online Service for InSAR (<http://ceg-research.ncl.ac.uk/v2/gacos/>) can be considered to integrate these corrections into our early warning system.

As we explained in section 3.1, the selection of points around the GPS stations is done by a distance criterion. All measured points that enter within that zone are chosen and no other parameters are currently taken into account. The existence of some parameter that gave us the quality of the measured points to take it into account when choosing or discarding the points involved in the calculation of the deformations in the area around the GPS stations, would allow us to improve the validation process.

REFERENCES

- Anguita et al. (2000). The Canary Islands origin: a unifying model. *Journal of Volcanology and Geothermal Research*, 103 1-26.
- Becerril et al. (2013). Spatial probability distribution of future volcanic eruptions at El Hierro Island (Canary Islands, Spain). *Journal of Volcanology and Geothermal Research* 257 (2013) 21–30
- Benito-Saz M.A., Parks, M.M., Sigmundsson, F., Hooper, A., García-Cañada, L. (2017) Repeated magmatic intrusions at El Hierro Island following the 2011–2012 submarine eruption. *J. Volcanol. Geotherm. Res.* 344:79–91. doi: 10.1016/j.jvolgeores.2017.01.020
- Becerril, L., Ubide, T., Sudo, M., Martí, J., Galindo, I., Galé, C., Morales, J.M., Yepes, J., Lago, M., Geochronological constraints on the evolution of El Hierro (Canary Islands), *Journal of U-Geohaz D3.8: VEW validation*

- African Earth Sciences (2015), doi: 10.1016/j.jafrearsci.2015.10.012.
- Béjar-Pizarro, M., Socquet, A., Armijo, R., Carrizo, D., Genrich, J., Simons, M., 2013. Andean structural control on interseismic coupling in the North Chile subduction zone. *Nat. Geosci.* 6, 462–467
- Biggs, J., Ebmeier, S. K., Aspinall, W. P., Lu, Z., Pritchard, M. E., Sparks, R. S. J., & Mather, T. A. (2014). Global link between deformation and volcanic eruption quantified by satellite imagery. *Nature Communications*, 5, 3471–3471. <https://doi.org/10.1038/ncomms4471>
- Biggs, J., & Pritchard, M. E. (2017). Global volcano monitoring: What does it mean when volcanoes deform? *Elements*, 13(1), 17 – 22. <https://doi.org/10.2113/gselements.13.1.17>
- Darias y Padrón, D.V., 1929. Noticias generales históricas sobre la isla de El Hierro. Imprenta Curbelo, La Laguna de Tenerife, p. 497.
- Doin, M., Lasserre, C., Peltzer, G., Cavalie, O., and Doubre, C. (2009). Corrections of stratified tropo- spheric delays in SAR interferometry: Validation with global atmospheric models. *J. Appl. Geophys.*, 69:35–50.
- Dzurisin D. (2003). A comprehensive approach to monitoring volcano deformation as a window on the eruption cycle, *Rev. Geophys.*, 41(1), 1001, doi:10.1029/2001RG000107.
- Carracedo JC, Badiola ER, Guillou H, Nuez JDL, Pérez Torrado FJ (2001) Geology and volcanology of La Palma and El Hierro, Western Canaries. *Estud Geol* 57:175–273
- García, A., A. Fernandez-Ros, M. Berrocoso, J.M. Marrero, G. Prates, S. De la Cruz-Reyna and R. Ortiz (2014). Magma displacements under insular volcanic fields, applications to eruption forecasting: El Hierro, Canary Islands, 2011-2013, *Geophys. J. Int.*; doi:10.1093/gji/ggt505.
- García-Cañada L. (2013) Different deformation patterns using GNSS in the volcanic process of El Hierro (Canary Island) 2011-2013. *EGU general Assembly Conference Abstracts*, pag 15791.
- Garthwaite MC, Miller VL, Saunders S, Parks MM, Hu G and Parker AL (2019) A Simplified Approach to Operational InSAR Monitoring of Volcano Deformation in Low- and Middle-Income Countries: Case Study of Rabaul Caldera, Papua New Guinea. *Front. Earth Sci.* 6:240. doi: 10.3389/feart.2018.00240
- Gee MJR, Watts AB, Masson DG, Mitchell NC (2001) Landslides and the evolution of El Hierro in the Canary Islands. *Mar Geol* 177:271–293. doi: 10.1016/S0025-3227(01)00153-0
- Hanssen, R. (2001). *Radar Interferometry, Data Interpretation and Error Analysis*. Kluwer Academic Publishers.

- Instituto Nacional de Estadística (INE) (2018) Cifras oficiales de población resultantes de la revisión del Padrón municipal a 1 de enero
- Klügel A. (2015) Deep intrusions, lateral magma transport and related uplift at ocean island volcanoes, *Earth and Planetary Science Letters*, Volume 431, 1 December 2015, Pages 140-149, ISSN 0012-821X, <http://dx.doi.org/10.1016/j.epsl.2015.09.031>.
- Li, Z., Fielding, E.J., Cross, P., Muller, J.P., 2006b. Interferometric synthetic aperture radar atmospheric correction: GPS topography-dependent turbulence model. *J. Geophys. Res. Solid Earth* 111 (B2).
- López, C. Et al. (2012). Monitoring the volcanic unrest of El Hierro (Canary Islands) before the onset of the 2011–2012 submarine eruption. *Geophys. Res. Lett.* 39, 7.
- Longpré, M.A., A. Klügel, A. Diehl and J. Stix (2014). Mixing in mantle magma reservoirs prior to and during the 2011-2012 eruption at El Hierro, Canary Islands, *Geology*; doi:10.1130/G35165.1.
- Loughlin, S. C., Sparks, R. S. J., Brown, S. K., Jenkins, S. F., & Vye-Brown, C. (2015). *Global volcanic hazards and risk*. Cambridge, United Kingdom: Cambridge University Press.
- Martí J, Ablay GJ, Bryan S (1996) Comment on ‘ The Canary Islands : an example of structural control on the growth of large oceanic-island volcanoes’ by J.C. Carracedo. *J Volcanol Geotherm Res* 72:143–149. doi: 10.1016/0377-0273(95)00079-8
- Martí, J., V. Pinel, C. López, A. Geyer, R. Abella, M. Tárraga, M.J. Blanco, A. Castro and C. Rodríguez (2013). Causes and mechanisms of the 2011-2012 El Hierro (Canary Islands) submarine eruption, *J. Geophys. Res. Solid Earth*, 118, 823-839; doi:10.1002/jgrb.50 087.
- Meletlidis et al. (2015). New insight into the 2011-2012 unrest and eruption of El Hierro Island (Canary Islands) based on integrated geophysical, geodetical and petrological data. *ANNALS OF GEOPHYSICS*, 58, 5, 2015, S0546; doi:10.4401/ag-6754
- Morgan, W.J., 1972. Deep mantle convection plumes and plate motions. *Am. Assoc. Pet. Geol. Bull.* 56 (2), 203–213.
- Pinel, V., Poland, M. P., & Hooper, A. (2014). Volcanology: Lessons learned from synthetic aperture radar imagery. *Journal of Volcanology and Geothermal Research*, 289, 81–113.
- Potter et al. (2018). Challenges and Benefits of Standardising Early Warning Systems: A Case Study of New Zealand’s Volcanic Alert Level System. In C. J. Fearnley et al. volume “Observing the Volcano World.
- Schmincke, H.-U., 1982. Volcanic and chemical evolution of the Canary Islands. In: von Rad, U., et al. (Eds.), *Geology of the Northwest African Continental Margin*. Springer, Berlin, U-Geohaz D3.8: VEW validation

Heidelberg, pp. 273–306.

UN ISDR (2003) Terminology: basic terms of disaster risk reduction retrieved 25/08/2009, from <http://www.unisdr.org/eng/library/lib-terminology-eng%20home.Htm>

Walters, R.J., Elliott, J.R., Li, Z., Parsons, B., 2013. Rapid strain accumulation on the Ashkabad fault (Turkmenistan) from atmosphere-corrected InSAR. *J. Geophys. Res. Solid Earth* 118 (7), 3674–3690.